Title

Management Implications of Snowpack Sensitivity to Temperature and Atmospheric Moisture Changes in Yosemite National Park, CA

Journal

JAWRA Journal of the American Water Resources Association, 54(3)

ISSN

1093-474X

Authors

Roche, James W
Bales, Roger C
Rice, Robert
et al.

Publication Date

2018-06-01

DOI

10.1111/1752-1688.12647

Peer reviewed

Management implications of snowpack sensitivity to temperature and atmospheric-moisture changes in Yosemite National Park, CA

James W. Roche[1], Roger C. Bales[2], Robert Rice[3], Danny G. Marks[4]

[1]Yosemite National Park, USDOI National Park Service, P.O. Box 700W, El Portal, California 95318
[2]Sierra Nevada Research Institute, University of California Merced, 5200 Lake Street, Merced, California 95340
[4]USDA Agricultural Research Service Northwest Research Center, Boise, Idaho 83712

ABSTRACT

In order to investigate snowpack sensitivity to temperature increases and end-member atmospheric-moisture conditions, we applied a well-constrained energy- and mass-balance snow model across the full elevation range of seasonal snowpack using forcing data from recent wet and dry years. Humidity scenarios examined were constant relative humidity (high) and constant vapor pressure between storms (low). With minimum calibration, model results captured the observed magnitude and timing of snowmelt. April 1 SWE losses of 38, 73, and 90% with temperature increases of 2, 4, and 6°C in a dry year centered on areas of greatest SWE accumulation. Each 2°C increment of warming also resulted in seasonal snowline moving upslope by 300 m. The zone of maximum melt was compressed upwards 100-500 m with 6°C warming, with the range reflecting differences in basin hypsometry. Melt contribution by elevations below 2000 m disappeared with 4°C warming. The constant-relative-humidity scenario resulted in 0-100 mm less snowpack in late spring versus the constant-vapor-pressure scenario in a wet year, a difference driven by increased thermal radiation (+1.2 W m^{-2}) and turbulent energy fluxes (+1.2 W m^{-2}) to the snowpack for the constant-relative-humidity case. Loss of snowpack storage and potential increases in forest evapotranspiration due to warming will result in a substantial shift in forest water balance and present major challenges to land management in this mountainous region.

Key Terms: snow hydrology; Sierra Nevada; simulation; watershed management

INTRODUCTION

Changes in snowpack profoundly affect ecological processes in mountainous regions, including annual evapotranspiration, stream flow and peak timing, wetland health, and wildlife (McMenamin *et al.*, 2008; Stewart *et al.*, 2005; Trujillo *et al.*, 2012). Western North America is projected to experience warming of 2-6°C (Representative Concentration Pathways 2.6 to 8.5 W m^{-2}) by the end of this century (Diffenbaugh and Field, 2013) and the impact that this will have on regional snowpack has been shown in many publications (Bales *et al.*, 2006; Dettinger *et al.*, 2004; Knowles and Cayan, 2004). Documented effects on snowpack over the past century (Andrews, 2012; Mote *et al.*, 2005) that are projected to continue growing in the future include decreased annual peak snow water equivalent (SWE) (Barnett *et al.*, 2005), increased winter runoff as snow transitions to rain (Stewart *et al.*, 2004), earlier annual snowpack disappearance (Brown and Mote, 2009), and negative glacial mass balance (Moore *et al.*, 2009).

There is a need for land managers to understand how changes in snowpack associated with the ongoing warming of the earth's climate affect forest health and fire, wildlife populations, and recreation (e.g. Flint *et al.*, 2013). Specifically, there is a need to understand in fine-grained spatial and temporal detail how snowpacks may change, and the factors that may mitigate that change, in order to develop management responses that address ecological transitions necessary for at-risk populations (e.g. Hannah *et al.*, 2014). Moreover, in order to be ecologically relevant, estimates of snowpack changes should be done at the watershed scale, including the entire rain-to-snow transition zone that usually contains the largest areas of resources of concern. In this zone, the shift from snow to rain precipitation and concomitantly reduced snowpack depth and duration will profoundly affect the rate and timing of water delivery to soils, which in turn will affect plant-available water in forest, wetland, riparian, and aquatic habitats during the snow-free season (Bales *et al.*, 2006; Schimel *et al.*, 2002).

The work of Sproles *et al.* (2012) and Cooper *et al.* (2016) illustrate the challenges of applying physically based snow models over large watersheds in the Pacific Northwest. These challenges include sparse instrumentation with which to drive models and to validate or evaluate results, and the methods chosen to distribute point

data spatially. Application of these models often requires substantial calibration in order to fit observed conditions at snow pillows or snow courses. Similar works by Flint *et al.* (2013) and Curtis *et al.* (2014) employ the SNOW-17 model, a hybrid empirical and physically based model (Anderson, 2006). Both methods rely heavily on the assumption that calibrations necessary to achieve results that match observed conditions do not affect representation of physical processes under future conditions that are beyond the range of variation for which the model was calibrated. There remains a persistent need to fully evaluate the effect of model calibration on internal energy dynamics and how this may affect warming-scenario results. An alternative approach is to physically model the snowpack without calibration, potentially sacrificing a better model fit to observations for more-consistent physics under warmer-climate scenarios. Research reported in this paper builds on prior work by using a full snow energy- and mass-balance model with minimal calibration to estimate the sensitivity of snowpack to temperature changes in wet and dry years.

Most snowpack or watershed modeling efforts assume constant relative humidity, implying increasing specific humidity with a warming climate, reflecting the ability of warmer air to hold more water vapor and in line with global land trends (Dai, 2006). In contrast, Pierce *et al.* (2013) predicted decreases in relative humidity over the western United States due to temperature increases outpacing atmospheric-moisture increases as the climate warms. Feld *et al.* (2013) demonstrated that errors in dew point temperature of +/-2°C advanced/extended the snow disappearance date by 3 days in the snow-dominated Tuolumne Meadows watershed in 2005, a relatively wet year with late-melting snow. The extent of the modeled change they observed was muted by offsetting changes in latent heat release through sublimation and longwave atmospheric radiation. Despite the small changes modeled by Feld *et al.* (2013), a necessary extension of their work is the examination of snow accumulation and melt patterns under different atmospheric moisture assumptions over entire watersheds and for the full range of expected temperature increases.

Three main questions motivated the research. First, by how much will snowpack storage across the current snow-covered elevation range change under mid- to end-of-century projected warming? Second, how robust are estimated changes to different model assumptions about atmospheric moisture? Third, what are the implications for ecosystem water availability in wet and dry years?

METHODS

We used *iSnobal*, a full energy- and mass-balance snowpack numerical model (Marks *et al.*, 1998; Marks *et al.*, 1999b) with minimal calibration to examine the sensitivity of snowpack to uniform temperature increases, and high and low estimates of future atmospheric moisture. Specifically, we examined the impact of assuming constant relative humidity (a high estimate of increased atmospheric moisture consistent with the observations of Dai (2006)) and constant vapor pressure (a low estimate of constant atmospheric moisture), between storms. Model results were compared to available snowpack measurements. Forcing data were then perturbed by uniform temperature increases, energy components recalculated for each atmospheric-moisture scenario, and the energy-balance model rerun. Results were compared to the base model, and relative differences in snowpack energy-balance components evaluated.

Study area

This investigation centered on the Merced and Tuolumne River basins in the central Sierra Nevada of California above their respective foothills dams, Exchequer and Don Pedro (Figure 1). The area comprises the broad western slope of the range, with elevations ranging from 100 to 3400 m, and encompassing all of Yosemite National Park. Much of the area receiving snowfall (>1500 m) is conifer dominated (73%), with shrubs, bare rock, and alpine tundra making up the rest of the area. Average annual precipitation from 800-m PRISM 1981–2010 climatology (PRISM Climate Group, Oregon State University, 2012) for the Merced and Tuolumne watersheds is 1060 and 1150 mm, respectively. Both basins are part of the San Joaquin River basin and comprise major sources of water for agriculture and municipalities. These basins were chosen for this study because they were sparsely instrumented, similar to others in the region, and because of the need to develop high-resolution climate-scenario products for Yosemite National Park and downstream stakeholders, including water districts and municipal utilities.

Model description

We ran the model *iSnobal* for water years 2011 and 2013 (beginning October 1st of the previous year), larger and smaller years with respect to average snowpack accumulation and total precipitation. *iSnobal* is a spatially distributed full-energy-balance snowpack model that is part of the Image Processing Workbench (IPW, Frew, 1990; Marks *et al.*, 1999a), a collection of computationally efficient raster processing and environmental physics calculation tools. Inputs to *iSnobal* are spatial arrays of hourly air temperature, vapor pressure, wind speed, soil temperature, long-wave radiation, net solar radiation, precipitation amount, precipitation temperature as determined by dew-point temperature, percentage of precipitation that is snow, and its density. The model calculates snowpack depth, density, temperature, melt, and energy balance as well as net radiative, turbulent, and advective energy fluxes. *iSnobal* is a compact numerically efficient representation of snowpack physics with minimal parameterization and as such is a valuable tool for examining snowpack sensitivity to available model inputs. After examining model results with respect to available observations, we then subjected these two model years to climate scenarios with uniform temperature increases of +2, +4, and +6°C and high and low atmospheric-humidity conditions.

Data

Terrain data were derived from a 100-m digital elevation model sampled from the 1/3 arc-second (~ 10 m) USGS National Elevation Dataset product that yielded a model domain of 1107 by 1296 cells. These data were used to derive slope, aspect, and sky-view fraction layers. Vegetation indices, including height and canopy light penetration, were derived from the U.S. Forest Service 30-m CALVEG (US Forest Service, 2014) geodatabase (hereafter referred to as CALVEG). This layer was resampled to 100-m resolution and aligned to the model grid using nearest-neighbor sampling.

Forcing data for the model were derived from ground-based measurements and supplemented by modeled inputs for the base water years of 2011 (wet) and 2013 (dry). We used a total of 34 weather stations within and immediately adjacent to the Merced and Tuolumne watersheds (Figure 1 and Table 1) that record on an hourly basis. Sites were operated by the California Department of Water Resources (DWR), Western Regional Climate Center (WRCC), National Interagency Fire Center Remote Automatic Weather Stations (RAWS), or Scripps Institution of Oceanography (SIO). Subsets of these stations were chosen for each input parameter based on knowledge of station locations and data type and quality. Each record was inspected for data continuity and coherence with adjacent stations; and gaps were filled using linear interpolation for periods of a few hours and linear regression with a nearby station for longer gaps.

A study objective was to examine snowpack sensitivity to temperature and humidity changes, and we chose stations that recorded both quantities where the authors were confident in the quality of the data due to knowledge of sensor maintenance (Figure 1, Table 1). Relative-humidity sensors are particularly prone to drift after one to two years and require regular recalibration for accurate measurements. RAWS stations listed in Table 1 received documented maintenance and recalibrated sensors on an annual or biannual basis. SIO stations received a comparable level of maintenance. Other stations such as the Dana Meadows site (DWR) were known by the authors to have been maintained properly for the two model years examined here.

Other station data used included precipitation, solar radiation as an indication of cloudiness, wind speed and direction, and various measures of snowpack used for model-performance evaluation. Precipitation data were derived from eleven stations that recorded both rain and snow accumulation, though notably only two sites were located at the highest elevations and both were rain-shadow affected. Solar radiation recorded at five (WY2011) and six (WY2013) stations with minimal tree and terrain shadowing were used to develop a spatial estimate of cloudiness. Wind-speed data recorded at seven relatively open locations were used to develop spatial wind-speed distributions. Wind direction was derived from a single station (Crane Flat Lookout) and no attempt was made to adjust these values given very limited data on wind direction and highly variable terrain. Twenty-two snow-course and eight snow-pillow locations, distributed snow-depth data from four locations along the Tioga Road, and snow LiDAR data from 2013 were used to also assess spatial model performance (Table 2).

Methods used to develop the gridded data inputs for *iSnobal* are detailed in the following paragraphs.

Precipitation. Hourly precipitation grids were generated using data from eleven stations that were first distributed using a modified inverse distance weighting (IDW) and then bias-corrected using daily 800-m resolution PRISM (PRISM Climate Group, Oregon State University, 2012) values. We used an IDW approach that averages weights based on distances to closest stations and distances to stations with the closest monthly PRISM values. This step minimizes the bullseye effect of simple IDW (with so few available stations) while being more computationally efficient that other methods such as co-kriging. These hourly precipitation grids were then bias-corrected using daily 800-m resolution PRISM data, using a simple delta approach. Average annual bias was -10.4 and -48.4 mm in dry and wet years, respectively. The proportion of precipitation falling as snow and its density were determined using dew-point temperature thresholds, as developed by Marks et al. (1999b).

Temperature and vapor pressure. Air and dew-point temperature (calculated using IPW) were distributed spatially on an hourly basis using detrended kriging (Garen *et al.*, 1994). For each hour, station values and elevation were linearly regressed and the resulting trend removed from the data. Residuals were then spatially kriged using a linear variogram and the elevation trend added back in. In the case where the regression slope was positive (increasing temperature with elevation), data were distributed using ordinary kriging only. Spatial grids of dew-point temperature were converted to vapor pressure, then to relative humidity, restricting values to 0–100%. To insure internal consistency, vapor pressure and dew point were then recalculated using these relative-humidity spatial fields with air temperature.

Net solar radiation. Hourly solar radiation input to the snowpack was calculated in a manner similar to that of Garen and Marks (2005). The IPW function stoporad (Dozier, 1980) was used to estimate theoretical clear-sky incoming global and diffuse visible (0.28-0.7 µm) and infrared (0.7-2.8 µm) radiation using atmospheric parameters adjusted to match measured clear-sky values at Dana Meadows. Stoporad adjusts these values based on solar zenith and azimuth angles and topographic slope, aspect, and shading from surrounding terrain. Resulting clear-sky grids of visible and infrared, diffuse and beam (global – diffuse) radiation were then adjusted for cloudiness, canopy, and albedo.

Clear-sky radiation was attenuated by cloudiness, estimated as the ratio of measured all-wave solar radiation to the calculated estimate of clear-sky values. We developed hourly ratios at six stations spanning the model domain where topographic and forest-canopy shading was minimal or could be reasonably corrected. Night-time cloud factors were estimated as an interpolation between the last daylight hour minus one hour and the first daylight hour plus one hour. All values were maximized to 1.0.

Next, attenuation due to forest canopy was estimated using the methods of Link *et al.* (2004) using adjusted parameters from Garen and Marks (2005). Pixels were classified as conifer, mixed conifer and hardwood, hardwood, or open based on CALVEG to match those used by the foregoing references (Table 3). Tree height was estimated using diameter at breast height values in CALVEG and an empirical fit for central Sierra Nevada forests from Zhao *et al.* (2012). Final values assigned to each grid cell were adjusted by the proportion of canopy-covered area from CALVEG.

Finally, estimated snowpack albedo was obtained using the method of Marshall and Warren (1987) as applied by Marks *et al.* (1999b) in the IPW albedo function. Albedo decay was determined at each model pixel based on the time since last snowfall (greater than 50% of precipitation) exceeding 0.5 mm water equivalent and accounting for solar-illumination angle. A single set of albedo parameters was used to facilitate the application of the model in future climate scenarios (effective grain size of new snow of 300 µm, maximum grain radius from grain growth of 2000 µm, and effective contamination factor of 2.0). Results were snowpack visible and infrared albedos in the range 0.9 to 0.99 and 0.4 to 0.7, respectively, that were then applied equally to diffuse and beam components. Net solar radiation was then determined by summing visible-beam, visible-diffuse, infrared-beam, and infrared-diffuse components.

Thermal radiation. We estimated incoming thermal radiation using the methods of Garen and Marks (2005) by first determining clear-sky longwave radiation, and then adjusting for cloudiness and forest canopy. Down-welling

longwave radiation was determined using the IPW topotherm tool that uses air and dew point temperature and elevation (Marks and Dozier, 1979). Additional thermal input from clouds was estimated based on a relation between proportionalities of measured to clear-sky thermal radiation (*TRR*) versus measured to clear-sky solar radiation (*SRR*), the latter being the cloudiness index referred to in the solar-radiation section above (after Garen and Marks (2005)). We used a modified version of their equation based on further measurements at Reynolds Mountain East experimental catchment (Reba *et al.*, 2011a; Reba *et al.*, 2011b):

$$TRR = mSRR + b \qquad (1)$$

where $m = 0.5070$ and $b = 1.5552$. Thermal radiation was then adjusted for forest canopy using the same canopy transmissivity value used for solar radiation (Table 3) and estimating canopy temperature to be air temperature after the methods of Link and Marks (1999). While canopy temperature may substantially exceed air temperature (Pomeroy *et al.*, 2009) particularly in more open forests on south slopes in this region, no data existed to improve this estimate.

Wind speed and direction. We used hourly wind speed measured at six locations to create hourly raster grids using IDW to distribute values. The chosen locations are largely open and distributed across the domain. Wind direction was taken from one location (Crane Flat Lookout) and distributed uniformly. Given that one purpose of the investigation was to examine snowpack sensitivity to changes in vapor pressure, a detailed topographic analysis of wind direction was deemed unnecessary. Wind speed, however, was adjusted for upwind terrain and vegetation characteristics using the methods of Winstral *et al.* (2009). Minimum wind speed was set to 0.447 m s^{-1} for model stability. This value is considerably less than average forest wind speeds (1 m s^{-1}) and changes turbulent energy exchange very little.

Soil temperature. Soil temperature was set to a constant of 0°C at 50-cm depth after Marks and Dozier (1992). While some soil-temperature data existed for the modeled periods, the energy state of soil was not coupled to the snowpack in the available version of *iSnobal* and as such there was little justification to change this boundary condition. Equally, ground heat flux is a minor component of snowpack energy balance (Granger and Male, 1978; Link and Marks, 1999; Marks and Dozier, 1992).

Climate sensitivity analysis

In order to isolate the role of temperature and vapor-pressure changes on snow accumulation and melt, we conducted a restricted sensitivity analysis (e.g. Miller *et al.*, 2003; Rasouli *et al.*, 2015) using uniform temperature increases, while holding precipitation timing and amount, seasonal temperature variation, and solar radiation constant. It should be noted that this approach may result in an overall energy balance that differs from available high resolution climate products (e.g. Flint and Flint, 2014), though use of these products relative to a given base year would confound our ability to examine the impacts of temperature and humidity variability on snowpack. Uniform temperature increases were also necessary to examine the effects of changes to base-year hourly forcing data and to avoid making assumptions about the magnitude of changes in minimum and maximum daily temperatures, during storm and non-storm periods, across highly variable mountain terrain. Finally, the sensitivity approach addresses management needs by using more intuitive temperature thresholds that are useful for current and future planning needs.

We perturbed air-temperature by creating rasters that were 2, 4 and 6°C greater than those used in the water years 2011 (wet) and 2013 (dry) base-model runs. The chosen values are consistent with the range of downscaled end-of-century warming estimates for an 8.5 W m^{-2} representative concentration pathway such as the those from the Basin Characterization Model (Flint and Flint, 2014). Models representative of the range of future temperature variability give average December-January-February temperature increases for the Tuolumne and Merced watershed above 1500 m for the 2070-2099 period of +3.2 to +5.3°C (Community Climate System Model Version 4 (ΔT_{min} = +2.7°C, ΔT_{max} = +3.6°C); Model for Interdisciplinary Research on Climate (ΔT_{min} = +4.2°C, ΔT_{max} = +6.4°C)).

The first humidity scheme consisted of assuming constant relative humidity, a common approach in climate modeling (Wigmosta *et al.*, 1994). This scheme effectively increased atmospheric moisture during all scenario model intervals. Model runs for this scheme were referred

to as RH2, RH4, and RH6 for the three temperature scenarios, respectively. From this, we recalculated vapor pressure and dew-point temperature, and then precipitation form, percent snow, and density. The change in dew point and precipitation then necessitated a recalculation of albedo, which is based on time since last snow. Thermal radiation was also recalculated given its dependence on air temperature and vapor pressure.

The second humidity scheme assumed that vapor pressure remained constant between storms (decreased relative humidity) and was sufficiently elevated during storms to achieve relative-humidity values consistent with the base model runs. To implement this, we set relative humidity to base-year values for the entire domain if any cell recorded precipitation. This simple approach was used given the synoptic nature of winter storms in the region. The latter step was necessary to retain physically real conditions during precipitation events where relative humidity was close to 100 percent and dew-point and air temperature were close in value. Model runs for this scenario were termed VP2, VP4, and VP6 for the respective temperature increases. Precipitation, albedo, and thermal-radiation grids were adjusted accordingly.

RESULTS

Base-year results were evaluated by comparing them to ground and LiDAR measurements. We then compared base-year and climate-scenario modeled snow accumulation and melt to assess warming effects across the elevation range of the basins. Additionally, we examined changes in energy forcing that affect the elevational patterns.

Base-year results and comparison to available measurements

Modeled snow depths compared favorably to the mean and standard deviation of snow-depth observations at distributed snow-sensor sites along the Tioga Road (Figure 2). Comparing model results with snow-pillow data showed a good match at the higher-elevation sites; however model performance was poorer at elevations below about 2400 m (Figure S1). It should also be noted that the highest snow pillow (Dana Meadows) was only 2990 m, leaving approximately 1000 m and 14% of the snow zone (Figure 1) above this elevation without snowpack measurements. Model predictions were also lower than most of the monthly snow-course values (Figure S2). In contrast to snow pillows, which have a footprint of a few meters, snow courses cover areas similar in size to the 100-m grid cell size used in the model, though parts of multiple model grid-cells overlie a snow course. Snow courses are largely in forest clearings, and typically have more snow than the surrounding forest. Lower model estimates at some locations may also be attributed to underestimates of precipitation amount in PRISM, particularly in WY2013 at Horse and Paradise Meadow sites, an issue highlighted by Henn *et al.* (2016). Nonetheless, the model produced results that approximate the magnitude and track the seasonal trend of snowpack, consistent with both dry and wet base years.

In contrast, modeled SWE was consistently higher than the experimental data product from the NASA Airborne Snow Observatory (Painter *et al.*, 2016) in 2013 (Figure S3). Snow depth was measured using laser altimetry during six flights in the spring of 2013 with the main product being a 50-m resolution estimate of snow depth and snow water equivalent (Painter *et al.*, 2016). These results were aggregated and aligned with the 100-m model grid using bilinear resampling. Results were compared by constructing boxplots of values in 300-m elevation bands. Despite our higher modeled SWE, elevational and season trends were similar to those of the ASO products.

Climate-sensitivity results

Substantial reduction of peak SWE was estimated in all warming scenarios, with the greatest reduction in areas that currently contribute the greatest amount of basin-wide SWE (Figure 3). Predicted dry-year SWE declined 38, 73, and 90% on April 1 for RH2, RH4, and RH6 scenarios, respectively (18, 56, and 85% in wet-year scenarios, not shown). Complete loss of the April 1 snowpack occurred in successive 300-m elevations bands with each 2°C warming. April 1snowpack exhibited the greatest declines at elevations centered around 2850 m (Figures 3 and S4). Integrated over the Merced and Tuolumne watersheds, peak SWE in the 2850-m band, which shifted earlier with warming, was reduced from base values in dry (wet) years by 38 (14)%, 55 (49)%, and 78 (73)% with 2, 4, 6°C warming (wet-year data not shown).

The sensitivity of peak SWE timing was substantially greater in dry versus wet year warming scenarios (Figure 4 and Table 4). In the

Merced basin, the date of peak SWE in a dry year shifted from mid-March to mid-January with 2°C of warming, and was about 200 mm lower (Figure 4). Melt rate was lower when compared to the base year and melt-out date was similar. Peak SWE shifted substantially in this case due to storm input early in the year, with little precipitation in February and March. The peak-SWE date shifted little in the +4 and +6°C cases, though the amount of SWE diminished by 100 then 125 mm with each 2°C increment of warming. Melt rates generally declined from 6.6 mm day^{-1} to 2-3 mm day^{-1} in dry-year scenarios and 11 mm day^{-1} to 7-10 mm day^{-1} in wet-year scenarios due to the earlier onset of melt. The +2, +4, and +6°C wet-year cases exhibited little change in peak SWE date from the base case (close to April 1st), with decreases of 250, 800, and 1250 mm SWE, respectively.

The rate of snowline retreat was similar for base and warming scenarios, though lower in the dry versus wet year scenarios (Figure 5). Melt-out date shifted 4-39 days at elevations above 3150 m for each 2°C warming in dry scenarios. Snowline retreat was approximately 9.9 m d^{-1} (12.6 m d^{-1}) in the base dry (wet) case, and 6.4-10.2 m d^{-1} (8.5-11.3 m d^{-1}) in dry (wet) warming scenarios. A change in the melt-out trend was evident around water year day 183 (April 1) in the dry scenarios, with snowline retreat before this date of 2.3-5.1 m d^{-1} and 8.0-18.8 m d^{-1} afterwards across all scenarios. A similar pattern was observed for the wet-year scenarios, though the change in melt rate occurred closer to water year day 240 (May 28).

A close correspondence between the elevation of peak annual melt and peak precipitation persisted in all warming scenarios for the Tuolumne Basin while progressively separating by several hundred meters in the Merced Basin (Figure 6). The zone of peak melt contribution contracted substantially and shifted approximately 500 m up in elevation in the Merced for the +6°C case compared to only 100-200 m for the Tuolumne. The contraction was more substantial in the Tuolumne case, with the top two 300-m melt-producing elevation bands exhibiting increased proportional melt contributions of 15-20% in contrast to the Merced (5-10%) and the wet-year case (10-15%). Base-year proportional melt contribution below 2000 m, the lower extent of the rain-snow transition zone, was approximately 10-15% and this largely disappeared once warming exceeded +2°C in both basins.

During the melt period, lower atmospheric moisture scenarios retained a slightly larger snowpack when compared to the constant-relative-humidity scenarios (Figure 7). For the +6°C, constant-relative-humidity scenario there was 50-100 mm less SWE during late winter and spring when compared to the constant-vapor-pressure scenarios, and melt-out 1-2 weeks earlier in elevation bands that produced the most melt. Differences increased with increasing snowpack – greater differences in the wet versus dry year scenarios – and between April and June. Differences were manifest primarily during melt due to the modeling assumption that relative humidity remained constant in the constant-vapor-pressure scenario when there was precipitation.

DISCUSSION

Accumulation and melt patterns

Examining individual wet and dry years and the impact of temperature changes revealed patterns that might be less apparent when averaging conditions over many years. The dry base year (2013) was highly sensitive to the rain-to-snow transition because it was warmer than 2011 and much of the annual snowpack arrived in a warm fall storm that accounted for over one-third of the peak SWE amount in the 2850-m elevation band (Figure 4). Warming of 2°C effectively removed this snowfall from the winter SWE balance. In contrast, the accumulation period in the cooler and wetter base year (2011) was less sensitive to +2°C warming because a greater percentage of the annual snowpack accumulated later and under colder conditions during a spate of late-December storms. Thus, in a warmer climate snow accumulation and spring melt patterns will be very sensitive to both the total precipitation and the amount of snowfall during the coldest winter months, versus warmer shoulder-season storms.

Melt rate also varied substantially between wet and dry year scenarios, corresponding to the season in which most melt occurred and the relative snow covered area. At the 2850-m band in 2013 (Figures 4 and 5, Table 4), peak snowmelt rates occurred between April 1 to June 1 (~8 mm d^{-1}) while substantially greater peak snowmelt rates were delayed until June 1 to August 1 during peak solar

insolation in 2011 (~20 mm d^{-1}). Warming shifted the period of peak melt rate earlier, greatly slowing overall melt rates, consistent with results shown by Musselman *et al.* (2017). Interestingly, melt rate for the +2°C wet year increased over the base year between April 1 and June 1 approaching that of the dry base year. Though the rate of melt per unit area of snow cover was greater in the 2013 base year, this is offset by the greater snow covered area in the 2011 RH2 scenario.

Basin hypsometry controlled the response of integrated annual melt to warming (Figure 6). In dry and wet base-year scenarios, more than half of melt originated from elevations above 2500 m, coincident with areas of elevated precipitation caused by orographic lifting of synoptic storm systems as they cross the mountain range. Peak proportional precipitation inputs in the snowmelt zone occurred at 2400 and 2800 m in the Merced and Tuolumne River watersheds, respectively, in both wet and dry years, which correspond to peak fractional basin area (note that the peak proportional precipitation 100-m elevation band for the Merced basin actually occurs below the seasonal snowpack zone at 1000 m). Precipitation contributions above these elevations drop off due to a combination of reduced basin area and rain-shadow effects. Warming scenarios shifted the elevation of the peak-melt contribution upwards by 17-83 m $°C^{-1}$, with larger shifts modeled in the Merced than the Tuolumne watershed. This is due to the proportionally greater area above 2800 m in the Tuolumne than Merced (17 vs 11%) snow zone. So, while warming caused upward shifts in the zone of peak melt in the Merced, the primary effect in the Tuolumne was to amplify the base-year melt peak, as lower elevations had rain instead of snow.

Sensitivity to humidity scenarios was only 10% that of temperature increases (Figures 7 and S5). Higher-atmospheric-moisture scenarios (RH2, RH4, RH6) exhibited faster melt-out rates than the respective low-humidity scenarios (VP2, VP4, VP6). Energy balance in the 2850-m band differed by +0.9 W m^{-2} from February 1 to May 1 between RH6 and VP6 wet-year scenarios, driven by greater net thermal radiation (+1.2 W m^{-2}) and turbulent-energy fluxes to the snowpack (+1.2 W m^{-2}). In contrast, increasing air temperature by 2°C increased the energy flux to the snowpack by 8.3 W m^{-2}, a difference driven by changes in thermal radiation, with smaller latent heat changes showing up in April and May (Figure 8). Solar radiation (net) to the snowpack is higher for the base model case in May and June due to greater proportional shading of the snowpack for the warmer scenario (energy components were averaged over areas with snowcover only).

Comparison of the 2013 model results to the Airborne Snow Observatory (ASO) snow LiDAR SWE product highlights the challenges of comparing spatial results to ground-based measurements (Figure S3). Model results underestimate SWE at ground-measurement locations (Figures S1, S2) and generally over-predict SWE when compared to the spatially continuous ASO product (Figure S3). The latter uses snow density derived from an *iSnobal* model that uses different temperature and precipitation forcing data than that used here (Hedrick et al., submitted). Further, comparison of model or ASO results to snow-course and snow-pillow data is inherently limited by uncertainty in measurement location, and the spatial resolution and quality of forcing data. While beyond the scope of this investigation, further evaluation of ASO and modeled results relative to improved ground measurements is a critical research area.

Limitations of modeling approach

Because the purpose of this study was to examine snowpack sensitivity to management-relevant climate-warming scenarios, limitations that impact this analysis must be noted. As a case study that examines only two winters using fixed temperature increases, this analysis can only capture trends specific to the temperature and precipitation patterns of the base water years. As computational expediency of the model improves (e.g. Havens *et al.*, 2017), one could extend this analysis to many different years and examine results for years that fall in between the early/dry and late/wet precipitation years in our analysis. Examining changes with respect to individual water years does, however, force careful consideration of unique effects such as individual storm temperature and timing that might otherwise be obscured in a larger, aggregated analysis.

The accuracy of results is largely limited by the accuracy of the forcing data. The snow model *iSnobal* is independent of the required forcing data – it does not calculate forcing parameters internally – and has been shown to very accurately simulate spatial patterns of snow cover development and

ablation (Garen and Marks, 2005; Kormos *et al.*, 2014; Kormos *et al.*, 2017; Marks *et al.*, 1998; Marks *et al.*, 1999b; Marks and Winstral, 2001; Marks *et al.*, 2001; Marks *et al.*, 2002; Nayak *et al.*, 2012). Precipitation timing, as distributed using inverse-distance weighting, may result in mismatches with dew-point records, resulting in changes in the rain-to-snow transition. This was particularly acute at lower elevations during early fall storms in the 2013 dry-year base-case modeling. Further, precipitation amount is quite uncertain in these basins as described by Henn *et al.* (2016) and illustrated by snow pillow totals that exceed the estimated precipitation for Horse Meadow in 2011 and 2013 (Figure S1). Ascribing a single set of albedo parameters limited the interpretation of results because it does not adequately account for enhanced albedo decay with the addition of late-season litter and dust accumulation at the snowpack surface (Hardy *et al.*, 2000; Hardy *et al.*, 2004). There was considerable uncertainty in the estimate of longwave radiation given a lack of measured values, which is a common issue in snowpack modeling (Lapo *et al.*, 2015; Raleigh *et al.*, 2015). While we did not incorporate canopy interception of snow, evidence suggests that evaporation or sublimation from tree canopies in humid temperate mountain areas is minimal (Storck *et al.*, 2002). Addressing uncertainty in all of these parameters and the resultant impact on results will be a fruitful avenue of research as computational efficiency of the model improves, and was beyond the scope of the present study. Model results are nonetheless useful for evaluation of snowpack sensitivity to climate change at a mountain watershed scale, and this effort plus its limitations highlight avenues for snowpack model improvement over large sparsely instrumented watersheds.

Management implications

Study results are instructive to water and forest management in these and similar mountain basins in that they provide an indication of potential snowpack reduction and loss with respect to location and progressive warming. Results suggest that the Tuolumne Meadows area at 2600 m elevation loses much of its snowpack by April 1 under a 4°C increase in a dry year and by April 1 under a 6°C increase in a wet year. Indeed, under these scenarios, the area known for its winter beauty and recreation will shift to a rain-dominated system by mid- to late-century. The meadow wetland environment that has excluded conifers is supported by late snowpack that in turn generates high groundwater levels well into the dry summer months. Once contributing-basin snowmelt ceases, groundwater levels drop quickly, leaving only a small amount of water in the upper layers of organic-rich meadows soils (Loheide II *et al.*, 2009). Loss of seasonal snow cover may lead to desiccation and loss of carbon from meadows (Arnold *et al.*, 2014) and decreased hydroperiod essential to maintaining wetland conditions that exclude trees (Lowry *et al.*, 2011), creating the potential to convert meadows to forest, as has been observed already in many mountain meadows in the west (Fites-Kaufman *et al.*, 2007; Millar *et al.*, 2004).

Reduced snowpack storage will affect water availability for downstream users, especially for communities dependent on run-of-the-river water systems where groundwater resources are limited (Lundquist and Roche, 2009). Water supply for the community of Wawona is derived from the South Fork Merced near the southern border of Yosemite National Park, and will likely be substantially affected by snowpack reduction. Model results suggest that the basin may lose approximately 50% of current April 1 snowpack with a 2°C temperature increase relative to the dry base year (Figure 3) and nearly all April 1 snowpack with a 4°C warming. Water-use restrictions imposed during recent drought years, of which 2013 was one, will likely become part of normal operations, with new restrictions becoming increasingly necessary as the length of the snow-free season increases. Downstream municipalities and agricultural operations that depend on streamflow in the Merced and Tuolumne Rivers will progressively lose snowpack storage (174 mm or 1.16×10^9 m^3 on April 1, 2013) equivalent to 31% of the combined primary rim dam reservoir capacity: Lakes McClure and Don Pedro on the Merced and Tuolumne Rivers, respectively.

SWE scenarios can be combined with evapotranspiration scenarios to estimate changes in the basin-wide water balance. For example, using the relation in Figure 4 of Goulden and Bales (2014), warming of 4°C would increase evapotranspiration by 179 mm per year, which when combined with a mean annual precipitation of

694 mm and estimated evapotranspiration of 510 mm in 2013 effectively eliminates runoff (Bales *et al.*, 2018). Snowpack storage on April 1 would be reduced from 171 mm to 46 mm implying that virtually all runoff will be derived from snowmelt. Vegetation management to reduce evapotranspiration will be essential to mitigating effects of increased temperature. Reducing biomass through forest thinning is possible on up to 25% of U.S. Forest Service lands given economic, access, and administrative constraints (North *et al.*, 2015). Remaining areas (U.S. Forest Service and National Park Service) would have to be thinned through managed fire (North *et al.*, 2015), which shows promise of increased or at least sustained water yield (Boisramé *et al.*, 2016).

Fine-scale snow-model results may assist managers in anticipating forest-fire activity. Lutz *et al.* (2009) documented an inverse relation between the number of fire starts and fire severity in Yosemite National Park and April 1 SWE in Tuolumne Meadows. This observation may reflect the duration of the snow-free period across elevations spanning the mixed-conifer zone (approximately 1500-2400 m), which may in turn determine vegetation and fuel dryness, as well as increased summer convective-storm activity, leading to increased lightning. Using the 300-m elevation band centered at 2550 m in the Tuolumne basin as a proxy for Lutz *et al.* (2009) Tuolumne Meadows SWE estimates, we found that modeled SWE declined by 38% (48%) in the wet (dry) year case for the 2°C warming scenario. Further warming of +4°C and +6°C resulted in April 1st SWE declines of 69% (86%) and 92% (100%) respectively for wet (dry) year cases examined in this study. This corresponds to advances in the average melt-out date in the 1500–2400 m elevation range from 44 days in the wet year scenario for +2°C (Figure 5) to complete snowpack loss in the lowest elevation bands in the +2 and +4°C dry year warming scenarios (Figures 5 and 6). Model results suggest avenues for refinement of the Lutz *et al.* (2009) analysis that may result in a more spatially-refined examination of forest fire susceptibility.

Quality precipitation measurements, particularly at high elevations, are essential to water management in a changing climate. Precipitation estimates derived from snow pillow records will become less reliable as the proportion of rain increases. For this study and the PRISM precipitation data used, there were only three (2013) or four (2011) precipitation gauges in the snow zone, three of which were concentrated in a 400 m elevation band in rain-shadow-affected areas of the upper Tuolumne watershed and Walker watershed immediately to the east. Managing increased flood risks due to more rain and less snow, water storage in reservoirs, and natural resources will require a much-improved network of weighing or accumulation gauges capable of accurately measuring mixed precipitation.

CONCLUSIONS

For both wet and dry years, changes in snowpack accumulation and melt, and reduced snowpack storage, have significant implications for the region. First, snowpack storage on April 1 in a dry year declines 38, 73, and 90% for +2°C, +4°C, and +6°C warming, respectively, in the zone of current snow maximum accumulation. The seasonal snowline retreats upslope 300 m for each 2°C warming, and areas below 2000 m become snow free once warming reaches +4°C. Second, constant-vapor-pressure scenarios increase late-season snowpack up to 100 mm over constant-relative-humidity scenarios, suggesting one should consider both end-member atmospheric moisture conditions when modeling snowpack under warmer temperatures.

Finally, there are many implications for future management in Sierra Nevada watersheds including transformation of snow- to rain-dominated ecosystems, progressive loss of snowpack storage as a component of water supply, and forest management. Transformation of the snowy subalpine environment to one dominated by rain would allow for more recreational access in many areas of Yosemite National Park requiring year-round rather than seasonal management presence. Loss of seasonal snow cover may also affect animal and bird habitat, carbon storage, and local water supplies in the Sierra Nevada. Reduction of snowpack storage by 2050 could require an additional one billion cubic meters of downstream storage. Considering increases in evapotranspiration with rising temperatures, much of the annual runoff in dry years could be derived solely from dwindling snowpack storage. As a potential mediator of forest-fire potential, changes in snowpack duration could result in drier summer conditions that are more susceptible to lightning due to increased convective storm activity. Some of this drying could be offset

through forest thinning, whether mechanical or through managed fire, resulting in reducing evapotranspiration while potentially enhancing accumulation and retention of a seasonal snowpack.

Supporting Information.
Additional supporting information may be found online under the Supporting Information tab for this article: Figures that more fully detail model evaluation and results.

Acknowledgements.
Support for this research was provided by the Yosemite Conservancy, the Merced Irrigation District through the California Integrated Regional Watershed Management Program (IRWMP), the Southern Sierra Critical Zone Observatory (Grant number EAR-1331939), and the UC Office of the President's Multi-Campus Research Programs and Initiatives (MR-15-328473) through UC Water, the University of California Water Security and Sustainability Research Initiative.
We acknowledge the contributions of Drs. Scott Havens (Agricultural Research Service) and Adam Winstral (Swiss Federal Institute for Forest, Snow and Landscape Research) for their immense help with the implementation of *iSnobal* and to Xiande Meng and Esther Canal for their assistance with forcing data preparation.

LITERATURE CITED

Anderson, E. A., 2006. Snow accumulation and ablation model–SNOW-17. http://www.nws.noaa.gov/oh/hrl/nwsrfs/users_manual/part2/_pdf/22snow17.pdf

Andrews, E. D., 2012. Hydrology of the Sierra Nevada Network national parks: Status and trends. Natural Resource Report, NPS/SIEN/NRR-2012/500. National Park Service, Fort Collins, Colorado, 196p.

Arnold, C., T. A. Ghezzehei, and A. A. Berhe. 2014. Early spring, severe frost events, and drought induce rapid carbon loss in high elevation meadows. PloS one, 9(9), DOI: 10.1371/journal.pone.0106058.

Bales, R. C., M. L. Goulden, C. T. Hunsaker, M. H. Conklin, P. C. Hartsough, A. T. O'Geen, J. W. Hopmans and M. Safeeq. 2018. Mechanisms controlling the impact of multi-year drought on mountain hydrology. Scientific Reports 8, Article number: 690, DOI:10.1038/s41598-017-19007-0.

Bales, R. C., N. P. Molotch, T. H. Painter, M. D. Dettinger, R. Rice, and J. Dozier. 2006. Mountain hydrology of the western United States. Water Resources Research, 42(8), DOI: 10.1029/2005WR004387.

Barnett, T. P., J. C. Adam, and D. P. Lettenmaier. 2005. Potential impacts of a warming climate on water availability in snow-dominated regions. Nature, 438(7066), 303-309, DOI: 10.1038/nature04141.

Boisramé, G., S. Thompson, B. Collins, and S. Stephens. 2016. Managed Wildfire Effects on Forest Resilience and Water in the Sierra Nevada. Ecosystems, 20(4), 717-732, DOI: 10.1007/s10021-016-0048-1.

Brown, R. D. and P. W. Mote. 2009. The Response of Northern Hemisphere Snow Cover to a Changing Climate. Journal of Climate, 22(8), 2124-2145, DOI: 10.1175/2008JCLI2665.1.

Cooper, M. G., A. W. Nolin, and M. Safeeq. 2016. Testing the recent snow drought as an analog for climate warming sensitivity of Cascades snowpacks. Environmental Research Letters, 11(8), DOI: 10.1088/1748-9326/11/8/084009.

Curtis, J. A., L. E. Flint, A. L. Flint, J. D. Lundquist, B. Hudgens, E. E. Boydston, et al. 2014. Incorporating cold-air pooling into downscaled climate models increases potential refugia for snow-dependent species within the Sierra Nevada Ecoregion, CA. PloS one, 9(9), DOI: 10.1371/journal.pone.0106984.

Dai, A., 2006. Recent Climatology, Variability, and Trends in Global Surface Humidity. Journal of Climate, 19(15), 3589-3606, DOI: 10.1175/JCLI3816.1.

Dettinger, M., D. Cayan, M. Meyer, and A. Jeton. 2004. Simulated Hydrologic Responses to Climate Variations and Change in the Merced, Carson, and American River Basins, Sierra Nevada, California, 1900–2099. Climatic Change, 62(1), 283-317, DOI: CLIM.0000013683.13346.4f.

Diffenbaugh, N. S. and C. B. Field. 2013. Changes in Ecologically Critical Terrestrial Climate Conditions. Science, 341(6145), 486-492, DOI: 10.1126/science.1237123.

Dozier, J., 1980. A clear-sky spectral solar radiation model for snow-covered mountainous terrain. Water Resources Research, 16(4), 709-718, DOI: 10.1029/WR016i004p00709.

Feld, S. I., N. C. Cristea, and J. D. Lundquist. 2013. Representing atmospheric moisture content along mountain slopes: Examination using distributed sensors in the Sierra Nevada, California. Water Resources Research, 49(7), 4424-4441, DOI: 10.1002/wrcr.20318.

Fites-Kaufman, J. A., P. Rundel, N. Stephenson, and D. A. Weixelman. 2007. Montane and subalpine vegetation of the Sierra Nevada and Cascade ranges. *Terrestrial Vegetation of California*. University of California Press, Berkeley, CA, 456-501.

Flint, L. E. and A. L. Flint. 2014. California Basin Characterization Model: A Dataset of Historical and Future Hydrologic Response to Climate Change, (ver.

1.1, May 2017): U.S. Geological Survey Data Release, DOI: 10.5066/F76T0JPB.

Flint, L., A. Flint, J. Thorne, and R. Boynton. 2013. Fine-scale hydrologic modeling for regional landscape applications: the California Basin Characterization Model development and performance. Ecological Processes, 2(1), 1-21, DOI: 10.1186/2192-1709-2-25.

Frew, J. E., 1990. The image processing workbench. Doctoral dissertation, University of California at Santa Barbara, Santa Barbara, California.

Garen, D. C., G. L. Johnson, and C. L. Hanson. 1994. Mean areal precipitation for daily hydrologic modeling in mountainous regions1. Journal of the America Water Resources Association, 30(3), 481-491, DOI: 10.1111/j.1752-1688.1994.tb03307.x.

Garen, D. C. and D. Marks. 2005. Spatially distributed energy balance snowmelt modelling in a mountainous river basin: estimation of meteorological inputs and verification of model results. Journal of Hydrology, 315(1), 126-153, DOI: 10.1016/j.jhydrol.2005.03.026.

Goulden, M. L. and R. C. Bales. 2014. Mountain runoff vulnerability to increased evapotranspiration with vegetation expansion. Proceedings of the National Academy of Sciences, 111(39), 14071-14075, DOI: 10.1073/pnas.1319316111.

Granger, R. J. and D. H. Male. 1978. Melting of a Prairie Snowpack. Journal of Applied Meteorology, 17(12), 1833-1842, DOI: 10.1175/1520 0450(1978)017<1833:MOAPS>2.0.CO;2.

Hannah, L., L. Flint, A. D. Syphard, M. A. Moritz, L. B. Buckley, and I. M. McCullough. 2014. Fine-grain modeling of species' response to climate change: holdouts, stepping-stones, and microrefugia. Trends in ecology & evolution, 29(7), 390-397, DOI: 10.1016/j.tree.2014.04.006.

Hardy, J. P., R. Melloh, P. Robinson, and R. Jordan. 2000. Incorporating effects of forest litter in a snow process model. Hydrological Processes, 14(18), 3227-3237, DOI: 10.1002/1099-1085(20001230)14:18<3227::AID-HYP198>3.0.CO;2-4.

Hardy, J. P., R. Melloh, G. Koenig, D. Marks, A. Winstral, J. W. Pomeroy, et al. 2004. Solar radiation transmission through conifer canopies. Agricultural and Forest Meteorology, 126(3), 257-270, DOI: 10.1016/j.agrformet.2004.06.012.

Havens, S., D. Marks, P. Kormos, and A. Hedrick. 2017. Spatial modeling for resources framework (SMRF): A modular framework for developing spatial forcing data for snow modeling in mountain basins. Computers & Geosciences, 109, 295-304, DOI: 10.1016/j.cageo.2017.08.016.

Hedrick, A., D. Marks, S. Havens, M. Robertson, M. Johnson, M, Sandusky, H. Marshall, P. Kormos, K. Bormann, and T.H. Painter. Submitted. Direct insertion of NASA Airborne Snow Observatory-derived snow depth time-series into the iSnobal energy balance snow model. Water Resources Research.

Henn, B., M. P. Clark, D. Kavetski, A. J. Newman, M. Hughes, B. McGurk, et al. 2016. Spatiotemporal patterns of precipitation inferred from streamflow observations across the Sierra Nevada mountain range. Journal of Hydrology, DOI: 10.1016/j.jhydrol.2016.08.009.

Knowles, N. and D. Cayan. 2004. Elevational Dependence of Projected Hydrologic Changes in the San Francisco Estuary and Watershed. Climatic Change, 62(1), 319-336, DOI: CLIM.0000013696.14308.b9.

Kormos, P. R., D. Marks, J. P. McNamara, H. P. Marshall, A. Winstral, and A. N. Flores. 2014. Snow distribution, melt and surface water inputs to the soil in the mountain rain–snow transition zone. Journal of Hydrology, 519, Part A, 190-204, DOI: 10.1016/j.jhydrol.2014.06.051.

Kormos, P. R., D. Marks, F. B. Pierson, C. J. Williams, S. P. Hardegree, S. Havens, et al. 2017. Ecosystem Water Availability in Juniper versus Sagebrush Snow-Dominated Rangelands. Rangeland Ecology & Management, 70(1), 116-128, DOI: 10.1016/j.rama.2016.05.003.

Lapo, K. E., L. M. Hinkelman, M. S. Raleigh, and J. D. Lundquist. 2015. Impact of errors in the downwelling irradiances on simulations of snow water equivalent, snow surface temperature, and the snow energy balance. Water Resources Research, 51(3), 1649-1670, DOI: 10.1002/2014WR016259.

Link, T. E., D. Marks, and J. P. Hardy. 2004. A deterministic method to characterize canopy radiative transfer properties. Hydrological Processes, 18(18), 3583-3594, DOI: 10.1002/hyp.5793.

Link, T. and D. Marks. 1999. Distributed simulation of snowcover mass- and energy- balance in the boreal forest. Hydrological Processes, 13(14-15), 2439-2452, DOI: 10.1002/(SICI)1099-1085(199910)13:14/15<2439::AID-HYP866>3.0.CO;2-1.

Loheide II, S., R. Deitchman, D. Cooper, E. Wolf, C. Hammersmark, and J. Lundquist. 2009. A framework for understanding the hydroecology of impacted wet meadows in the Sierra Nevada and Cascade Ranges, California, USA. Hydrogeology Journal, 17(1), 229-246, DOI: 10.1007/s10040-008-0380-4.

Lowry, C. S., S. P. Loheide, C. M. Moore, and J. D. Lundquist. 2011. Groundwater controls on vegetation composition and patterning in mountain meadows. Water Resources Research, 47(10), DOI: 10.1029/2010WR010086.

Lundquist, J. and J. Roche. 2009. Climate change and water supply in western national parks. Park Science, 26(1), 31-33, Spring 2009, ISSN 1090-9966.

Lutz, J. A., J. W. Van Wagtendonk, A. E. Thode, J. D. Miller, and J. F. Franklin. 2009. Climate, lightning ignitions, and fire severity in Yosemite National Park, California, USA. International Journal of Wildland Fire, 18(7), 765-774, DOI: 10.1071/WF08117.

Marks, D., J. Domingo, and J. Frew. 1999a. Software tools for hydro-climatic modeling and analysis: Image processing workbench, ARS-USGS Version 2. *ARS Technical Bulletin NWRC-99-1*, 1

Marks, D. and J. Dozier. 1979. A clear-sky longwave radiation model for remote alpine areas. Archiv für Meteorologie, Geophysik und Bioklimatologie Serie B, 27(2-3), 159-187, DOI: 10.1007/BF02243741.

Marks, D., J. Domingo, D. Susong, T. Link, and D. Garen. 1999b. A spatially distributed energy balance snowmelt model for application in mountain basins. Hydrological Processes, 13(12-13), 1935 -1959, DOI: 10.1002/(SICI)1099-1085(199909)13:12/13<1935::AID-HYP868>3.0.CO;2-C.

Marks, D. and J. Dozier. 1992. Climate and energy exchange at the snow surface in the Alpine Region of the Sierra Nevada: 2. Snow cover energy balance. Water Resources Research, 28(11), 3043-3054, DOI: 10.1029/92WR01483.

Marks, D., J. Kimball, D. Tingey, and T. Link. 1998. The sensitivity of snowmelt processes to climate conditions and forest cover during rain-on-snow: a case study of the 1996 Pacific Northwest flood. Hydrological Processes, 12(10-11), 1569-1587, DOI: 10.1002/(SICI)1099-1085(199808/09)12:10/11<1569::AID-HYP682>3.0.CO;2-L.

Marks, D., T. Link, A. Winstral, and D. Garen. 2001. Simulating snowmelt processes during rain-on-snow over a semi-arid mountain basin. Annals of Glaciology, 32(1), 195-202, DOI: 10.3189/172756401781819751.

Marks, D. and A. Winstral. 2001. Comparison of Snow Deposition, the Snow Cover Energy Balance, and Snowmelt at Two Sites in a Semiarid Mountain Basin. Journal of Hydrometeorology, 2(3), 213-227, DOI: COSDTS>2.0.CO;2.

Marks, D., A. Winstral, and M. Seyfried. 2002. Simulation of terrain and forest shelter effects on patterns of snow deposition, snowmelt and runoff over a semi-arid mountain catchment. Hydrological Processes, 16(18), 3605-3626, DOI: 10.1002/hyp.1237.

Marshall, S. E. and S. G. Warren. 1987. Parameterization of snow albedo for climate models. In Large Scale Effects of Seasonal Snow Cover, B.E. Goodison, R.G. Barry, J. Dozier Eds. IAHS-AIHS Publication 166, International Association of Hydrological Sciences, Wallingford, UK, 43-50.

McMenamin, S. K., E. A. Hadly, and C. K. Wright. 2008. Climatic Change and Wetland Desiccation Cause Amphibian Decline in Yellowstone National Park. Proceedings of the National Academy of Sciences of the United States of America, 105(44), 16988-16993, DOI: 10.1073/pnas.0809090105.

Millar, C. I., R. D. Westfall, D. L. Delany, J. C. King, and L. J. Graumlich. 2004. Response of Subalpine Conifers in the Sierra Nevada, California, U.S.A., to 20th-Century Warming and Decadal Climate Variability. Arctic, Antarctic, and Alpine Research, 36(2), 181-200, DOI: 10.1657/1523-0430(2004)036[0181:ROSCIT]2.0.CO;2.

Miller, N. L., K. E. Bashford, and E. Strem. 2003. Potential impacts of climate change on California hydrology. JAWRA Journal of the American Water Resources Association, 39(4), 771-784, DOI: 10.1111/j.1752-1688.2003.tb04404.x.

Moore, R. D., S. W. Fleming, B. Menounos, R. Wheate, A. Fountain, K. Stahl, et al. 2009. Glacier change in western North America: influences on hydrology, geomorphic hazards and water quality. Hydrological Processes, 23(1), 42-61, DOI: 10.1002/hyp.7162.

Mote, P. M., A. F. Hamlet, M. P. Clark, and D. P. Lettenmaier. 2005. Declining Mountain Snowpack in Western North America. Bulletin of the American Meteorological Society, 86(1), 39-49, DOI: 10.1175/BAMS-86-1-39.

Musselman, K. N., M. P. Clark, C. Liu, K. Ikeda, and R. Rasmussen. 2017. Slower snowmelt in a warmer world. Nature Climate Change, 7, 214-219, DOI: 10.1038/nclimate3225.

Nayak, A., D. Marks, D. G. Chandler, and A. Winstral. 2012. Modeling Interannual Variability in Snow-Cover Development and Melt for a Semiarid Mountain Catchment. Journal of Hydrologic Engineering, 17(1), 74-84, DOI: 10.1061/(ASCE)HE.1943-5584.0000408.

North, M., A. Brough, J. Long, B. Collins, P. Bowden, D. Yasuda, et al. 2015. Constraints on mechanized treatment significantly limit mechanical fuels reduction extent in the Sierra Nevada. Journal of Forestry, 113(1), 40-48, DOI: 10.5849/jof.14-058.

Painter, T. H., D. F. Berisford, J. W. Boardman, K. J. Bormann, J. S. Deems, F. Gehrke, et al. 2016. The Airborne Snow Observatory: Fusion of scanning lidar, imaging spectrometer, and physically-based modeling for mapping snow water equivalent and snow albedo. Remote Sensing of Environment, 184, 139-152, DOI: 10.1016/j.rse.2016.06.018.

Pierce, D. W., A. L. Westerling, and J. Oyler. 2013. Future humidity trends over the western United States in the CMIP5 global climate models and variable infiltration capacity hydrological modeling system. Hydrology and Earth System Sciences, 17(5), 1833-1850, DOI: 10.5194/hess-17-1833-2013.

Pomeroy, J. W., D. Marks, T. Link, C. Ellis, J. Hardy, A. Rowlands, et al. 2009. The impact of coniferous forest temperature on incoming longwave radiation to melting snow. Hydrological Processes, 23(17), 2513-2525, DOI: 10.1002/hyp.7325.

PRISM Climate Group, Oregon State University, 2012. http://prism.oregonstate.edu.

Raleigh, M. S., J. D. Lundquist, and M. P. Clark. 2015. Exploring the impact of forcing error characteristics on physically based snow simulations within a global sensitivity analysis framework. Hydrology and Earth System Sciences, 19(7), 3153-3179, DOI: 10.5194/hess-19-3153-2015.

Rasouli, K., J. W. Pomeroy, and D. G. Marks. 2015. Snowpack sensitivity to perturbed climate in a cool mid-latitude mountain catchment. Hydrological Processes, 29(18), 3925-3940, DOI: 10.1002/hyp.10587.

Reba, M. L., D. Marks, M. Seyfried, A. Winstral, M. Kumar, and G. Flerchinger. 2011. A long-term data set for hydrologic modeling in a snow-dominated mountain catchment. Water Resources Research, 47(7), DOI: 10.1029/2010WR010030.

Reba, M. L., D. Marks, A. Winstral, T. E. Link, and M. Kumar. 2011. Sensitivity of the snowcover energetics in a mountain basin to variations in climate. Hydrological Processes, 25(21), 3312-3321, DOI: 10.1002/hyp.8155.

Schimel, D., T. G. Kittel, S. Running, R. Monson, A. Turnipseed, and D. Anderson. 2002. Carbon sequestration studied in western US mountains. Eos, Transactions American Geophysical Union, 83(40), 445-449, DOI: 10.1029/2002EO000314.

Sproles, E. A., A. W. Nolin, K. Rittger, and T. H. Painter. 2012. Climate change impacts on maritime mountain snowpack in the Oregon Cascades. Hydrology and Earth System Sciences Discussions, 9(11), 13037-13081, DOI: 10.5194/hessd-9-13037-2012.

Stewart, I. T., D. R. Cayan, and M. D. Dettinger. 2004. Changes in snowmelt runoff timing in western North America under a business as usual climate change scenario. Climatic Change, 62(1), 217-232, DOI: CLIM.0000013702.22656.e8.

Stewart, I. T., D. R. Cayan, and M. D. Dettinger. 2005. Changes toward earlier streamflow timing across Western North America. Journal of Climate, 18(8), 1136-1155, DOI: 10.1175/JCLI3321.1.

Storck, P., D. P. Lettenmaier, and S. M. Bolton. 2002. Measurement of snow interception and canopy effects on snow accumulation and melt in a mountainous maritime climate, Oregon, United States. Water Resources Research 38(11): 5-1 - 5-16. DOI: 10.1029/2002WR001281.

Trujillo, E., N. P. Molotch, M. L. Goulden, A. E. Kelly, and R. C. Bales. 2012. Elevation-dependent influence of snow accumulation on forest greening. Nature Geoscience, 5(10), 705, DOI: 10.1038/ngeo1571.

US Forest Service, 2014. Existing Vegetation - CALVEG, ESRI personal geodatabase. https://www.fs.usda.gov/detail/r5/landmanagement/resourcemanagement/?cid=stelprdb5347192.

Wigmosta, M. S., L. W. Vail, and D. P. Lettenmaier. 1994. A distributed hydrology-vegetation model for complex terrain. Water Resources Research, 30(6), 1665-1679, DOI: 10.1029/94WR00436.

Winstral, A., D. Marks, and R. Gurney. 2009. An efficient method for distributing wind speeds over heterogeneous terrain. Hydrological Processes, 23(17), 2526-2535, DOI: 10.1002/hyp.7141.

Zhao, F., Q. Guo, and M. Kelly. 2012. Allometric equation choice impacts lidar-based forest biomass estimates: A case study from the Sierra National Forest, CA. Agricultural and Forest Meteorology, 165, 64-72, DOI: 10.1016/j.agrformet.2012.05.019.

Table 1. Meteorological stations and data used to force model.

Station name[1]	Elev., m	UTM easting[2], m	UTM northing[2], m	Measurements used[3]	Operator[4]
Green Springs (GRN)	311	4193067	191966	t, rh, p	RAWS
Stanislaus Powerhouse (SPW)	333	4225930	204880	p	PGE
Cathey's Valley (CVR)	366	4151342	224905	t, rh, p	RAWS
Dudley Ranch (DUC)	366	4151264	224864	p	MID
Briceburg (MBB)	452	4165485	237083	p	MID
Mariposa (MRP)	680	4154996	235967	t, rh, p	RAWS
Priest Reservoir (PRR-SIO)	709	4189078	212647	t, rh	SIO
Metcalf Gap (MCF)	938	4143892	255011	t, rh	RAWS
Batterson (BTT)	943	4140575	268301	p	RAWS
Smith Peak (SEW)	1168	4188222	226980	sr, w	RAWS
Smith Peak (SEW-SIO)	1168	4188222	226980	t, rh	SIO
Jerseydale (JSD)	1189	4158967	249214	t, rh	RAWS
Hetch Hetchy (HEM)	1195	4203412	255489	p	HHWP
Wawona (WWN)	1235	4158119	265654	t, rh, sr	RAWS
Yosemite Valley (YYV)	1208	4181238	271843	p	MID
Miami Mountain (MIA)	1321	4144912	257059	t, rh, sr, w	RAWS
Sunset Inn (SUN-SIO)	1371	4188288	245001	t, rh	SIO
Hodgdon (HDG-SIO)	1397	4187075	248304	t, rh	SIO
Mount Elizabeth (MTE)	1504	4217791	215134	t, rh, sr, w	RAWS
Yosemite South Entrance (YOW)	1511	4154480	267291	p	MID
Forty Mile (FTY-SIO)	1723	4184565	247936	t, rh	SIO
Pinecrest (PNW)	1738	4230750	236322	t, rh, sr, w	RAWS
Merced Grove (MEG-SIO)	1810	4183446	249675	t, rh	SIO
Mariposa Grove (MPG)	1951	4154932	269754	t, rh	RAWS
Crane Flat (CFL-CRN)	2017	4182829	251510	p	NOAA
Crane Flat Lookout (CFL)	2026	4182878	251530	t, rh, sr, w	RAWS
Gin Flat (GIN-SIO)	2149	4183578	255577	t, rh	SIO
Fresno Dome (FRS)	2177	4149346	275698	t, rh, w	UCM
Smoky Jack (SMK-SIO)	2182	4188935	261192	t, rh	SIO
White Wolf (WHW)	2408	4193540	266732	t, rh, sr, w	RAWS
Olmsted Quarry (OLM-SIO)	2604	4187768	279089	t, rh	SIO
Tuolumne Meadows (TUM)	2622	4194700	293480	p	CA-DWR
Virginia Lakes Ridge (VRG)	2879	4215567	304085	p	NRCS
Dana Meadow (DAN)	2988	4196683	301507	t, rh, sr, w	CA-DWR

[1]Station name abbreviations: Three letter abbreviations are derived from conventions in the California Data Exchange Commission database (http://cdec.water.ca.gov/). Abbreviations ending with "-SIO" indicate stations operated by Scripps Institution of Oceanography that are not currently available through CDEC. CFL-CRN indicates the NOAA Climate Reference Network Station located near the Crane Flat Lookout.
[2]Geographic coordinates are in Universal Transverse Mercator (UTM) projection, North American 1983 Datum, Zone 11.
[3]Variable abbreviations: p, precipitation; rh, relative humidity; sr, solar radiation; t, air temperature; w, wind speed and direction.
[4]Operator abbreviations are: RAWS – Interagency Fire Remote Access Weather Station network managed by the Bureau of Land Management; SIO – Scripps Institution of Oceanography; UCM – University of California Merced; CA-DWR – California Department of Water Resources; MID – Merced Irrigation District; HHWP – Hetch Hetchy Water and Power; NRCS – Natural Resource Conservation Service; PGE – Pacific Gas and Electric; NOAA – National Oceanic and Atmospheric Administration Climate Reference Network.

Table 2. Snow data sources.

Station name[1]	Elev., m	UTM northing[2], m	UTM easting[2], m	Data type[3]
Merced Grove (MEG-SIO)	1810	4183446	249675	distributed snow depth
Bell Meadow (BEM)	1981	4228435	242260	monthly swe
Beehive Meadow (BHV)	1981	4208908	255883	monthly swe
Lower Kibbie (LKB)	2042	4213387	247407	monthly swe
Lake Vernon (VNN)	2042	4211186	261488	monthly swe
Upper Kibbie Ridge (UKR)	2042	4214521	246651	monthly swe
Kerrick Ranch (KRC)	2134	4229596	240718	monthly swe
Gin Flat (GFL)	2134	4183363	255739	monthly swe; hourly swe
Peregoy Meadow (PGM)	2134	4172111	268473	monthly swe
Smoky Jack (SMK-SIO)	2182	4188935	261192	distributed snow depth
Paradise Meadow (PDS)	2332	4214396	265710	monthly swe; hourly swe
Huckleberry Lake (HCL)	2377	4220692	259308	monthly swe
Spotted Fawn Lake (SPF)	2377	4219616	258135	monthly swe
Sachse Spring (SAS)	2408	4219048	251182	monthly swe
White Wolf (WHW)	2408	4193540	266732	hourly swe
Wilma Lake (WLW)	2438	4218298	269071	monthly swe
Tenaya Lake (TNY)	2484	4190665	284584	monthly swe; hourly swe
Ostrander Lake (STR)	2499	4168599	274999	monthly swe; hourly swe
Horse Meadow (HRS)	2560	4226695	266766	monthly swe; hourly swe
Olmsted Quarry (OLM-SIO)	2604	4187768	279089	distributed snow depth
Tuolumne Meadow (TUM)	2621	4194327	293307	monthly swe
Snow Flat (SNF)	2652	4189558	280239	monthly swe
New Grace Meadow (NGM)	2713	4225694	270684	monthly swe
Slide Canyon (SLI)	2797	4218724	286737	hourly swe
Bond Pass (BNP)	2835	4228817	270246	monthly swe
Rafferty Meadow (RFM)	2865	4190277	295406	monthly swe
Dana Meadow (DAN)	2987	4196789	301552	monthly swe, hourly swe

[1]See footnote 1 in Table 1.
[2]See footnote 2 in Table 1.
[3]Data type explanations: monthly swe denotes manually measured snow courses, hourly swe indicates a snow-pillow site, and distributed snow depth indicates sites with 4-6 snow depth sensors distributed across an area of approximately 100 meters square.

Table 3. Canopy parameters (adapted from Link and Marks 1999).

Vegetation class	tau (τ)	mu (μ)
Herbaceous, sparse shrub, non-vegetated	1	0
Conifer forest/woodland	0.2	0.040
Mixed conifer and hardwood	0.3	0.033
Hardwood forest/woodland	0.4	0.025

Table 4. Base and climate scenario summary snowpack results for the 300-meter elevation band centered at 2850 m in the Merced basin.[a]

Model run	Dry				Wet			
	Peak SWE mm	Peak day	Melt-out day	Melt rate mm d^{-1}	Peak SWE mm	Peak day	Melt-out day	Melt rate mm d^{-1}
Base	645	160	243	6.6	1484	181	307	10.9
RH2	400	107	223	2.6	1248	179	287	10.6
RH4	311	91	188	2.2	722	179	264	7.3
RH6	150	91	110	2.7	317	177	200	9.4
VP2	402	107	225	2.6	1262	179	292	10.3
VP4	312	91	195	2.0	755	179	270	7.2
VP6	151	91	112	2.4	340	177	212	6.9

[a] Day units are number of days since the start of the water year (October 1st). Melt-out day is the first day after peak SWE that snowpack falls below 100 mm SWE. Melt rate is the peak SWE minus 100 mm divided by the number of days between peak SWE and melt-out.

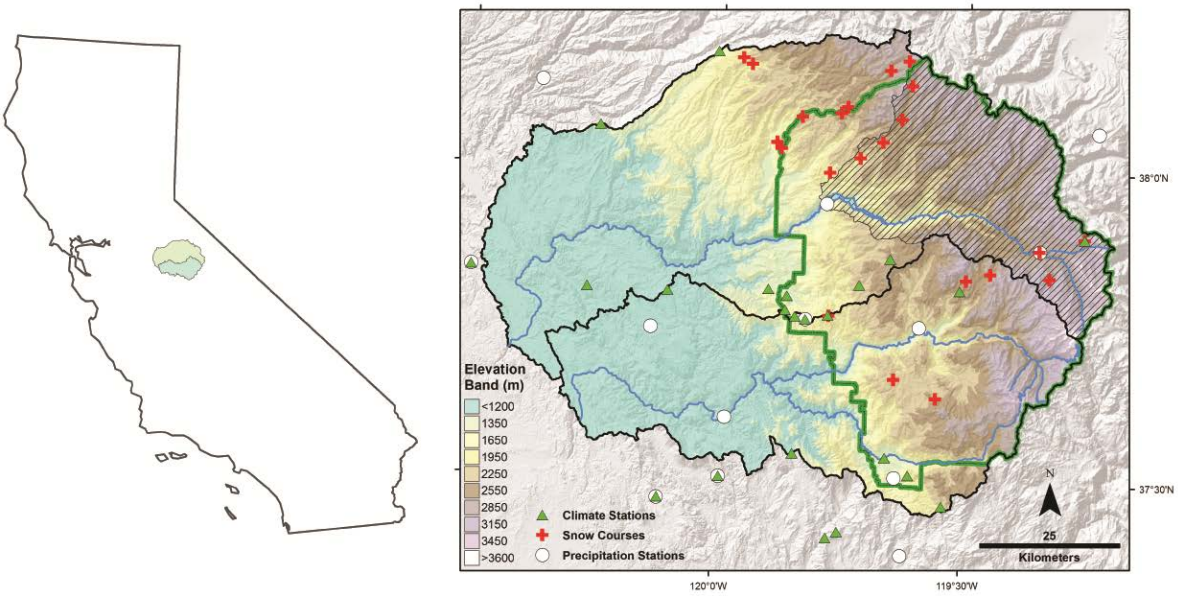

Figure 1. Merced and Tuolumne River watersheds in the central Sierra Nevada of California. Climate and precipitation stations used to force model runs are shown, along with snow courses used to evaluate model performance. Yosemite National Park is shown within a green border and diagonal hatching demarks the Hetch Hetchy watershed. The current approximate seasonal "snow zone" exists at elevations above the 1500 m contour.

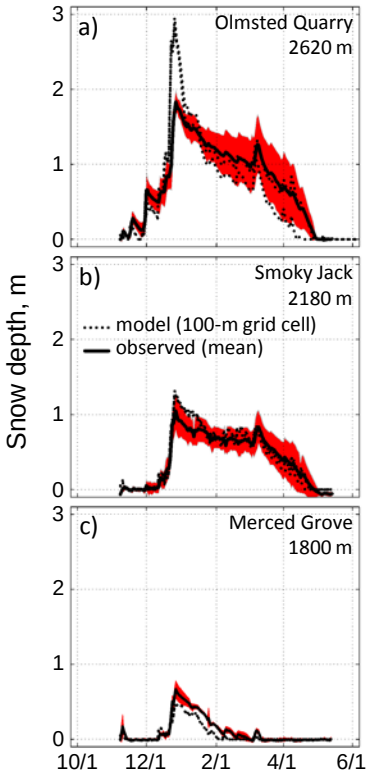

Figure 2. Modeled and observed snow depths at three distributed snow depth monitoring locations along an elevational transect for WY13. Shading indicates the standard deviation of observations. Each site had 4-6 operational sensors during the period shown. Each 100-m grid cell that overlapped sensor locations is depicted separately.

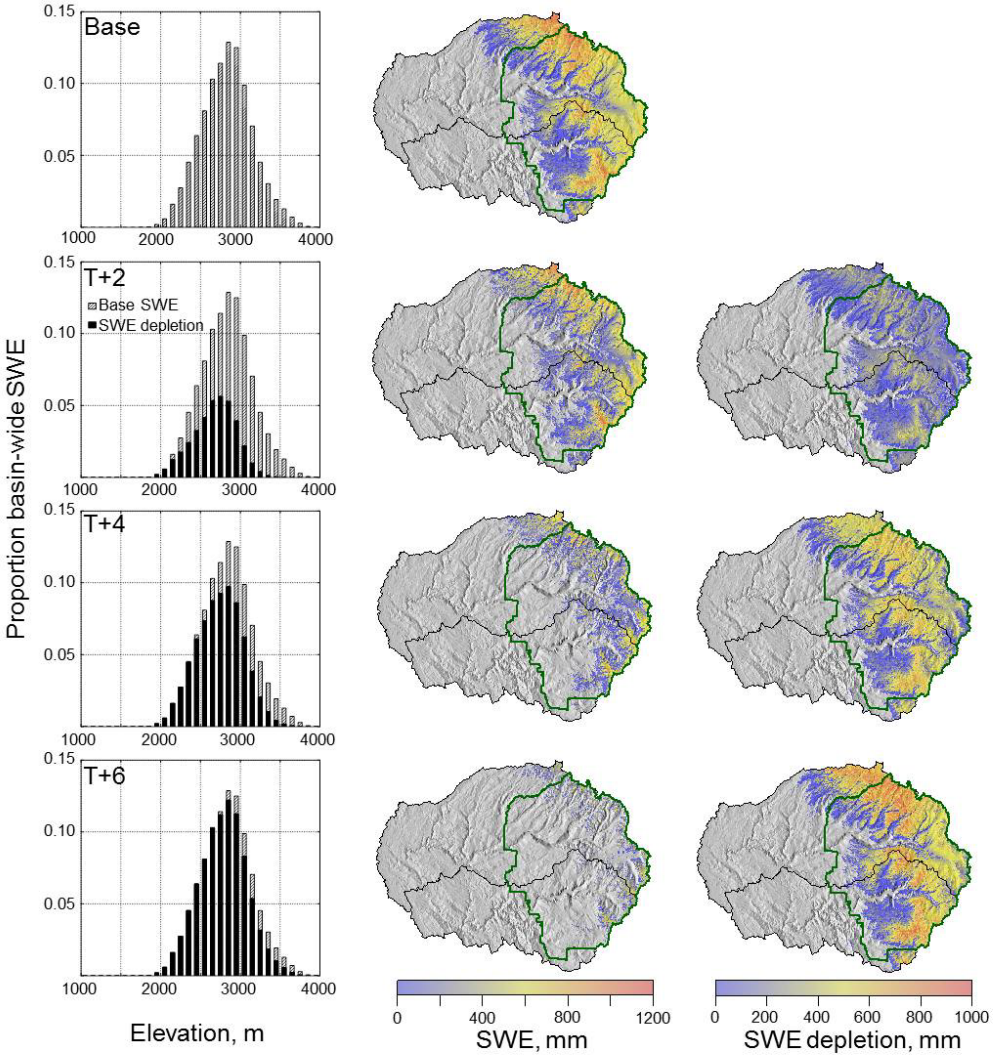

Figure 3. Proportion of basin-wide April 1 modeled snow-water-equivalent depletion in constant-relative-humidity temperature increase scenarios for water year 2013 by 100-m elevation band (left), modeled April SWE for each scenario (middle), and spatial absolute SWE depletion (right). Black outlines on watershed maps are the Tuolumne (northern part) and Merced (southern part) watersheds and the green outline is the boundary of Yosemite National Park.

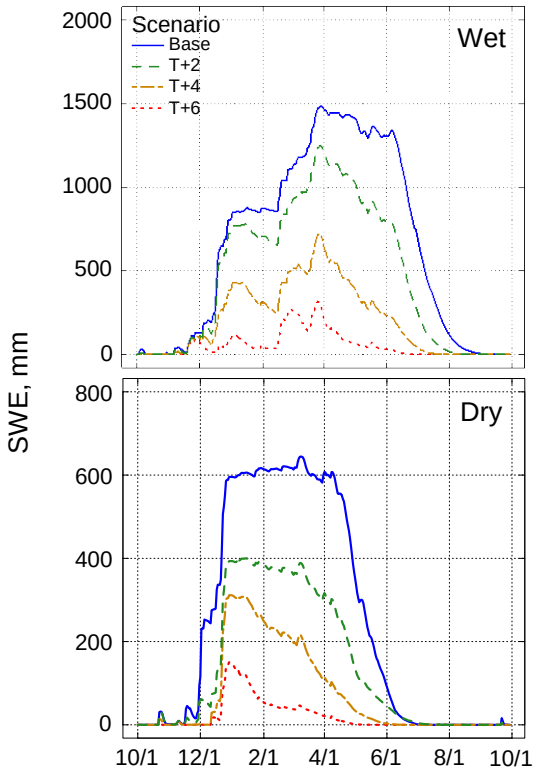

Figure 4. Snowpack evolution in the Merced River basin for base modeled wet (WY11) and dry (WY13) years as well as constant relative humidity scenarios (+2, +4, +6°C) for the 2850 m elevation band. Note the different ordinate scales. See Figure S4 for results for other elevation bands.

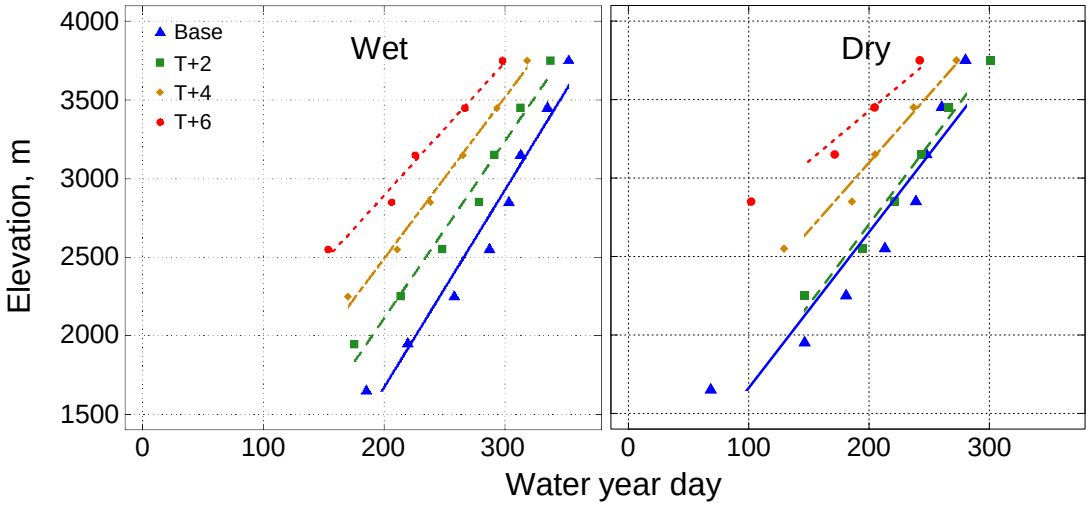

Figure 5. Melt-out day (average grid cell value < 100 mm SWE) by 300-m elevation band for base-case wet and dry years and constant-relative humidity warming scenarios in the Tuolumne River basin.

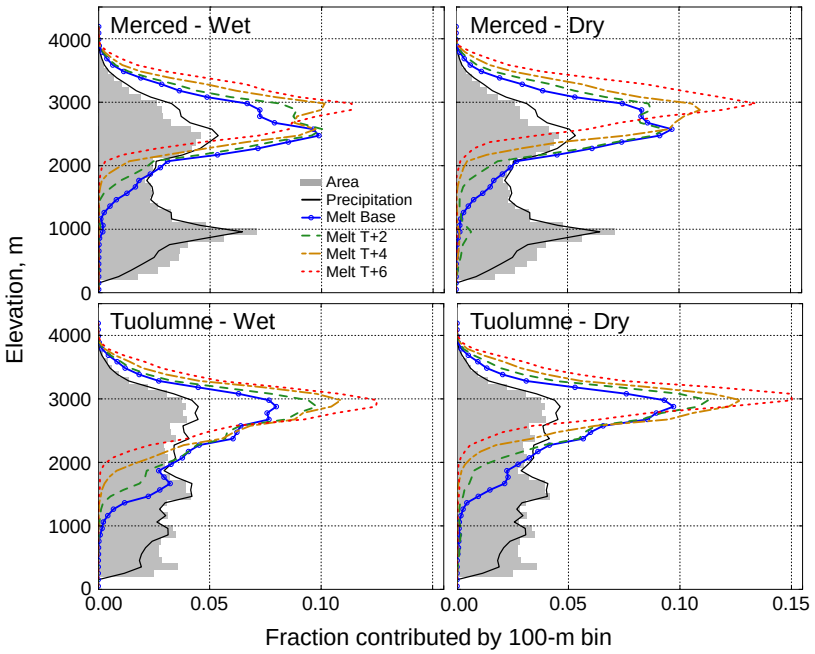

Figure 6. Elevational relationship of precipitation (model input) and fractional contribution to basin-wide snowmelt by basin area for base case and constant-relative-humidity temperature increase scenarios.

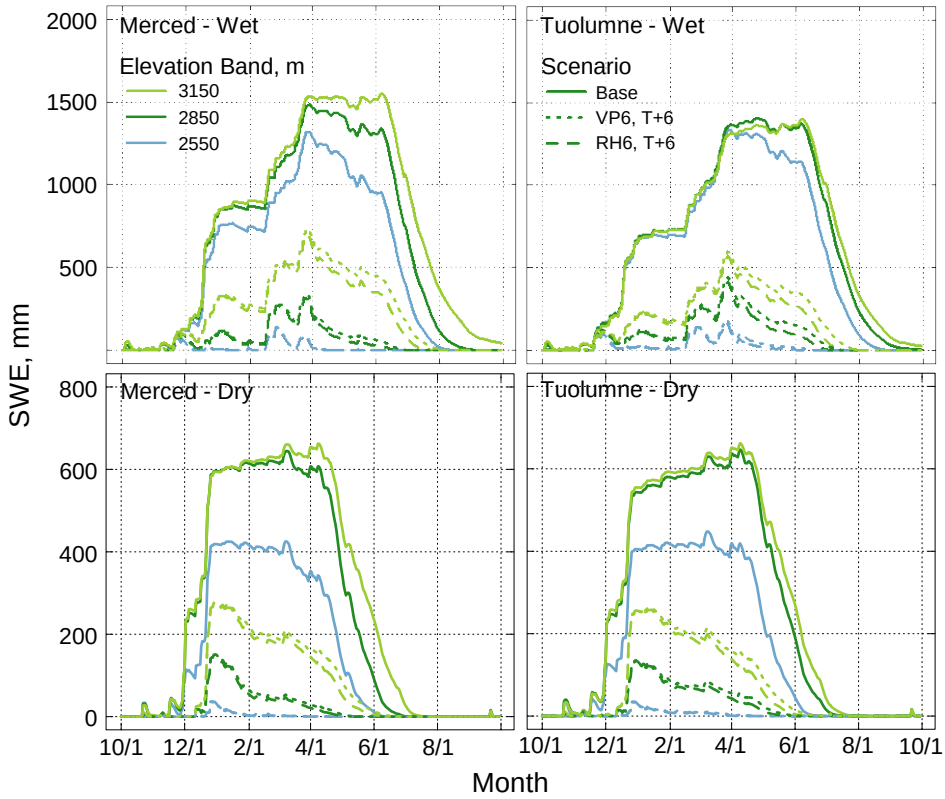

Figure 7. Seasonal snowpack progression for 300-m elevation bands that produce the most snowmelt in base and constant-relative-humidity and constant-vapor-pressure temperature increase scenarios. Note the difference in snow-water-equivalent scales between the wet and dry years. Full results for the Merced basin are shown in Figure S5.

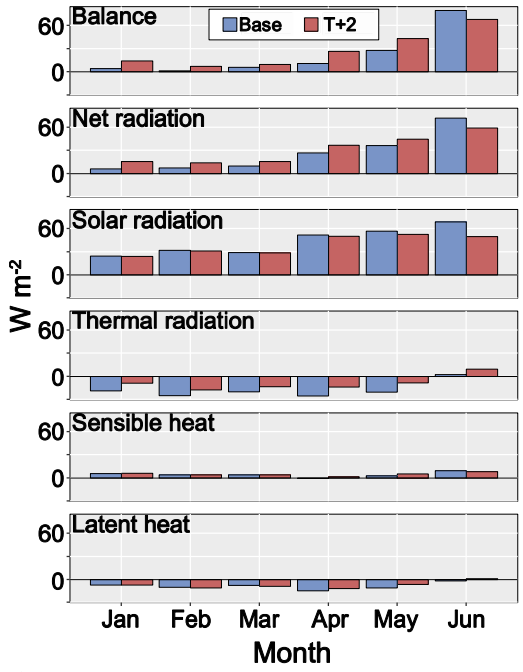

Figure 8. Energy balance for the 300-m elevation band centered on 2850 m in the Merced watershed for 2011 (wet base year) and a temperature increase of 2ºC with constant relative humidity (RH2 scenario). Energy components are as follows: snowpack energy balance, net all-wave radiation to the snowpack, net solar radiation, thermal or longwave radiation, sensible, and latent energy (positive toward the snow surface). Net energy to the snowpack in June is less for the RH2 scenario due to reduced net solar radiation to the snowpack.

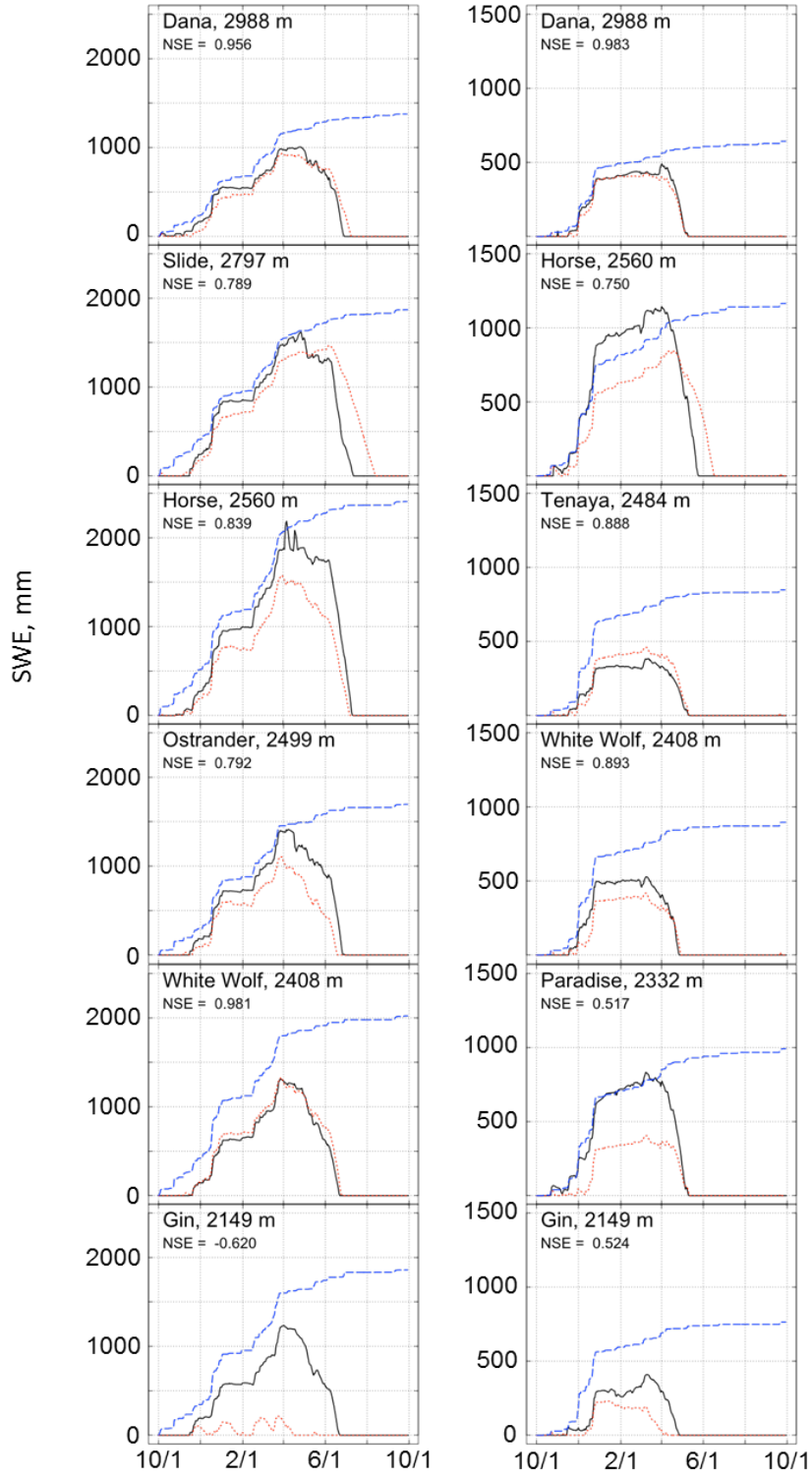

Figure S1. Observed (solid black) and modeled (dotted red) SWE at snow pillows Water Year 2011 (left) and 2013 (right). Dashed blue line depicts cumulative precipitation from daily 800 m PRISM dataset. NSE refers to the Nash-Sutcliffe coefficient indicating the level of agreement. Note different SWE scales for the two water years.

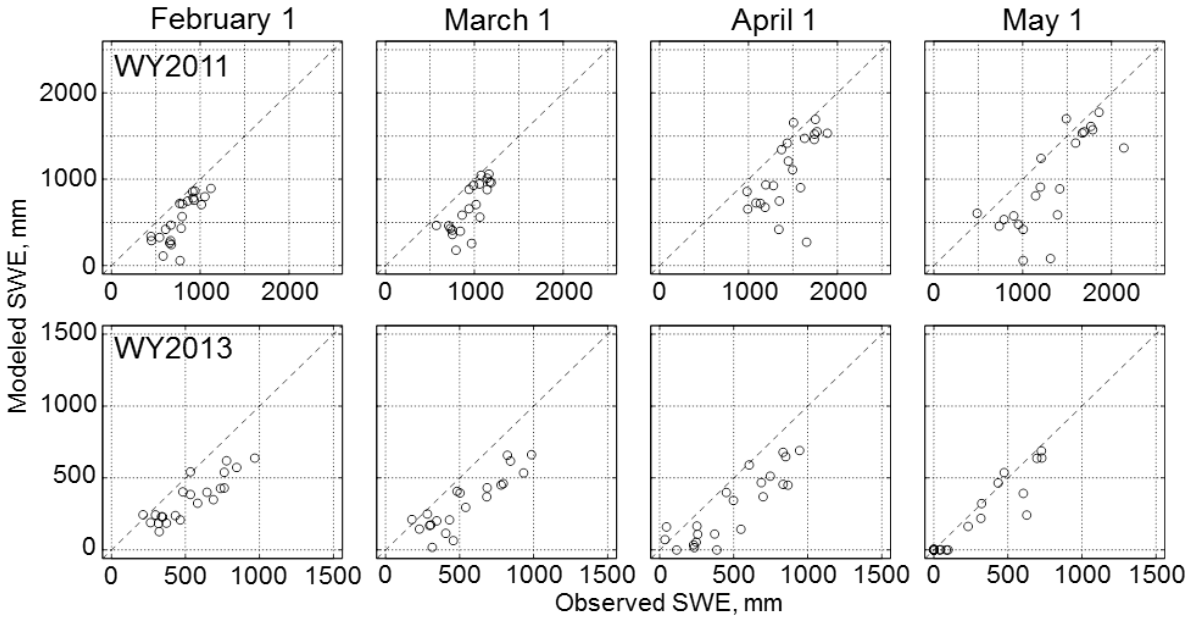

Figure S2. Observed and modeled SWE results at snow courses. See Table 2 for site information.

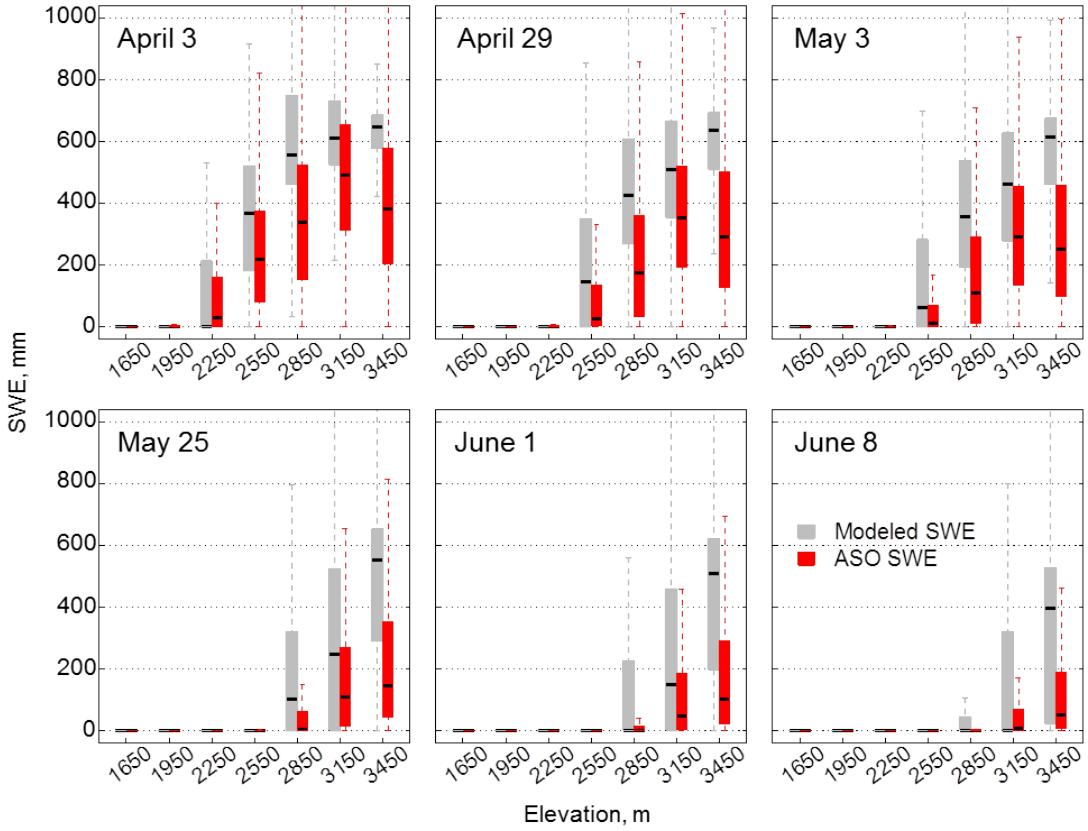

Figure S3. Box and whisker plots of modeled (gray) and NASA Airborne Snow Observatory derived SWE (red) by 300-m elevation bands in the Hetch Hetchy Watershed for water year 2013. Boxes span the 25th to 75th percentile values, with the black bar indicating the median and whiskers spanning the range of data.

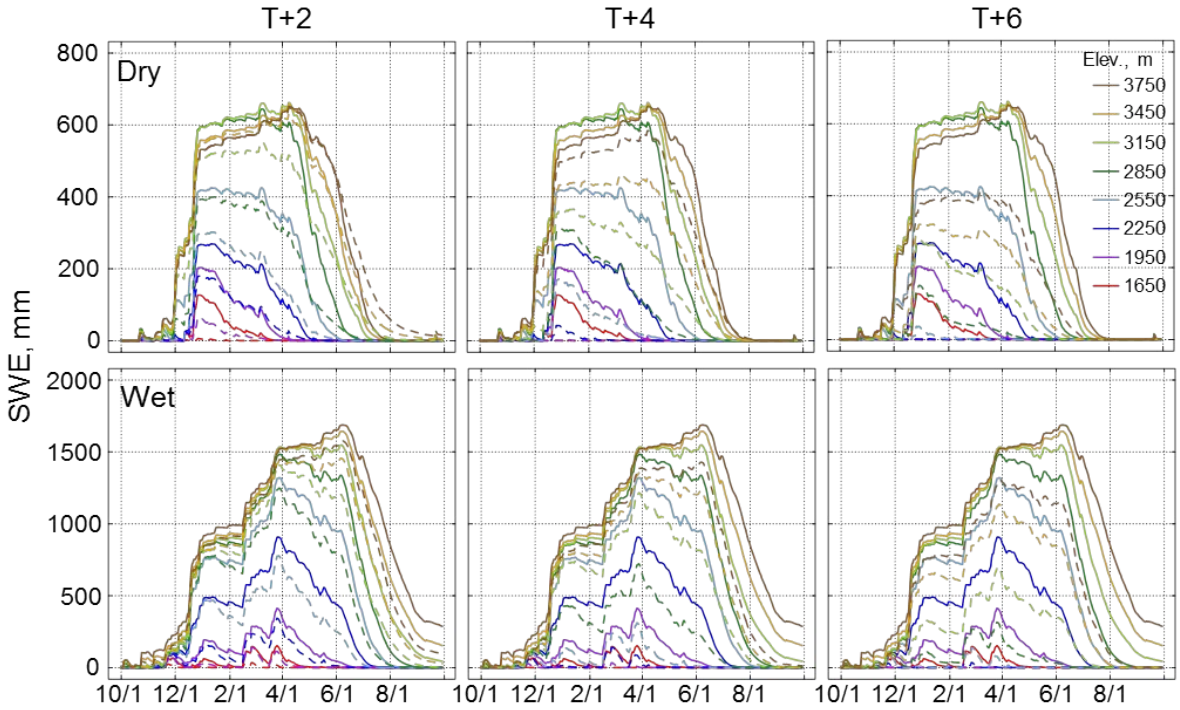

Figure S4. Snow water equivalent by 300-meter elevation band for base and climate scenarios in the Merced River basin. Solid Lines = Base model years (Dry = 2013, Wet = 2011) Dashed Lines = Constant-relative-humidity temperature increase scenarios.

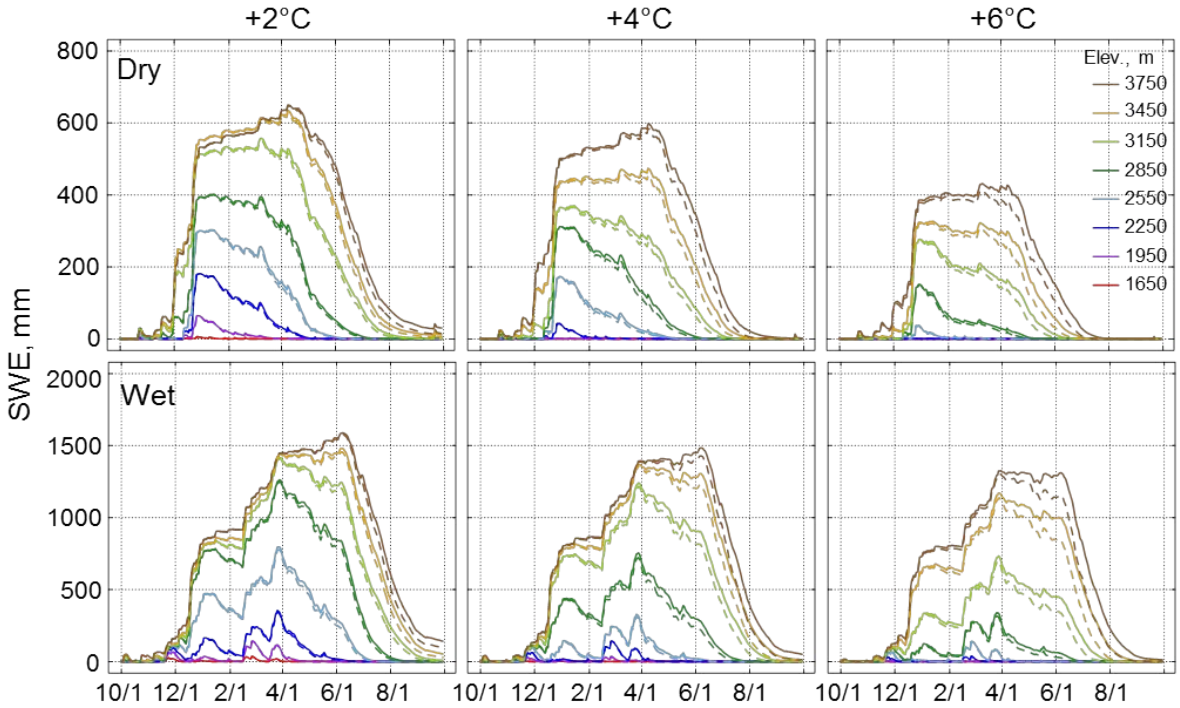

Figure S5. Modeled snow water equivalent by 300-meter elevation band comparing atmospheric moisture scenario results in the Merced River basin in dry and wet years. Solid Lines = Constant vapor pressure, Dashed Lines = Constant relative humidity.